Corrosion of API 5L X60 Pipeline Steel in Soil and Surface Defects Detection by Ultrasonic Analysis

Fatima Benkhedda [1], **Ismail Bensaid** [2], **Abderrahim Benmoussat** [1,*], **Sid Ahmed Benmansour** [1] and **Abdeldjelil Amara Zenati** [1]

1   Materials Research Team, LAEPO Research Laboratory, University of Tlemcen, Tlemcen 13000, Algeria; zohra200911@live.com (F.B.); benman65@yahoo.fr (S.A.B.); z_amara2000@yahoo.fr (A.A.Z.)
2   Materials Research and Structure Laboratory, University of Tlemcen, Tlemcen 13000, Algeria; bensaidismail@yahoo.fr
*   Correspondence: abbenmoussa@gmail.com

Abstract: The corrosion steels phenomenon is one of the main problems in the oil industry, such as in buried transmission pipelines used for high gas pressure for long distances. Steels are protected from the external soil corrosion through a bituminous coating, whose action is coupled with a cathodic protection system, which aims to maintain steel in its protection field and thus to avoid any corrosion risk. However, steels in service may experience external surface defects like corrosion pitting and cracking due to electrochemical or mechanical interactions of bare steel with an aggressive soil solution after steel protection failure. These are concerning phenomena and are the major threats of the pipeline transmission system's reliability and ecological safety. Corrosion mechanisms are varied and can be evaluated by different methods, such as electrochemical measurements, which are influenced by various factors like temperature, pH, soil characteristics, resistivity, water content, and as well mechanical stresses. Corrosion results from simulated artificial soil solutions showed that steel is sensitive to corrosion by soil. Surface defects detection was carried out using an ultrasonic non-destructive method such as C-Scan Emission testing and the time of flight diffraction technique (TOFD) ultrasonic non-contact testing method. After propagation of the ultrasonic waves, the diffracted ultrasonic reflected wave occurring at the edges of the defects appears due to the presence of a corrosion defect by generating defect echoes. The C-Scan ultrasonic image shows surface reflection, including corrosion defects on interfaces with varying acoustic impedances. The cross-transverse speed ultrasonic propagation through the plate including defect is modified, revealing more surface defects, and cross-transverse speed is shown to increase ultrasonic detection presents some advantages, such as precision and speed of detection without alteration to the structure. This method can be used in the industrial context as an intelligent industrial robotics technique.

Keywords: X60 steel; surface defect; corrosion pits; weld effect; soil corrosion; ultrasonic analysis; C-scan; TOFD

1. Introduction

API5L X60 steel tubes are used for gas transmission under pressure in pipeline due to their adequate mechanical properties and corrosion resistance. The steel is produced using a controlled factory cooling-based metallurgical scheme (TMCP—thermos mechanical controlled process) [1] by refining the ferritic grain size, increasing the yield strength and toughness achieved by various hardening mechanisms based on dislocation movement. The chemical composition and mechanical characteristics must meet the specified requirements and acceptance criteria according to API standards [2]. The chemical composition is specified as the maximum limit of four elements, carbon, manganese, phosphorus, and sulphur, which are used for the welded tubes. There are no cracks in any part of the pipe, and openings in the weld GZ1 40″ buried line are exploited by the Algerian Sonatrach

Company, developed in 1976, which consists of steel pipes of welded rolled type, with a depth between 0.6 and 1 m, protected from the external soil by a thick coating with bituminous binder and an active cathodic protection system (CP) applied on site at -850 mV $Cu/CuSO_4$ to isolate the steel from the soil environment and avoid any risk of degradation by corrosion or cracking.

Unfortunately, the steel line after over thirty years of service presents some external steel surface defects such as pitting corrosion, cracking, weld joint defects, etc. Most failures are caused by corrosion pitting. The points to consider in the study are to understand better the mechanisms of steel corrosion by soil and the influence of physical parameters such as temperature, pH, and immersion duration as well as the influence of mechanical stresses. In the second step, we search for adequate methods for detecting and characterizing surface defects. The process of steel corrosion by soils involves many physicochemical parameters such as soil composition, soil resistivity, and steel chemical composition. This is the result of the electrochemical interaction between the steel and the soil environment, returning to the more thermodynamically stable oxidized form. The damage process also includes many electrochemical and mechanical parameters. Default hazards, such as external chemical interactions are concerning phenomena in the oil industry and research laboratory. They are the major threats that can lessen the underlying integrity of the pipelines' transmission system. The corrosion profile is the consequence of coatings failure that does not have adequate cathodic protection, the main causes of which are defective soils. The effects of this corrosion result in losses of thickness at various depths, which may lead to perforation and gas leaks.

Many studies have been developed in recent years [3–12] with the aim of finding adequate anti-corrosion protection solutions in order to limit or remove them. Chemical composition is key to understanding how a soil can influence corrosion. It is necessary to examine every particular pipeline site to explain the corrosion mechanism models resulting from the steel interaction with the soil environment, which depends on numerous factors such as soil nature, moisture content, resistivity, and pH.

Authors of study [3] examined the corrosion of S235JR carbon steel for pipelines in artificial soil solution, focusing on water content, which is directly linked to other very influential parameters such as aeration or oxygen level, soil resistivity, and active surface area. The study dealt with the phenomena occurring during transitional periods of drying and wetting of several types of soil: clayey, clayey loam, and sandy. Electrochemistry was used to estimate corrosion rates by modeling voltammetry curves around the abandonment potential. The samples underwent analysis using Raman micro-spectroscopy, X-ray diffraction, and various microscopy techniques to determine the steel corrosion mechanisms. The results showed that in the case of high humidity and poor ventilation, corrosion rates are very low but become significant during the drying phases.

In study [4], the corrosion behavior of low-carbon pipeline steel in soil was studied by considering some soil parameters such as nature, resistivity, and physical parameters of low-resistivity soil, like montmorillonite clay, which exhibits corrosive properties that decrease with soil moisture content and temperature, facilitating ionic exchange between the steel surface and the corrosive soil environment. In soil corrosion, steel surface defects as a result of corrosion interactions are primarily related to the composition of the soil in which the pipeline is buried. The phenomenon is accentuated by decreasing pH values and increasing temperature.

The corrosion behavior of uncoated low-carbon steels such as X65 steel [5] was studied after burial in most real limestone soil. The samples were not catholically protected during gravimetric field testing. The results showed significant roughness and a change in color of the surface due to the presence of rust and lime deposits. The X65 steel was the most susceptible to corrosion, as tested by electrochemical methods in real limestone soil showing increased corrosion.

In [6], X80 pipeline steel was immersed in silty soil at different salinities and temperatures and was studied in corrosion by electrochemical methods. Results showed that in the

corrosive soil environment, with a concentration range of 0.3 to 2% NaCl, passive current densities increase with chloride ion concentration, and the soil becomes more corrosive at the maximum concentration. Ions present in the silty solution of soil pores cause differences in the corrosion behavior of X80 steel at different soil temperatures in the range of 263 to 283 K. Corrosion is more accentuated at higher temperatures. Soil parameters influence on pipeline steel corrosion behavior exposed in near-neutral pH soil simulating solution has been investigated by potentiodynamic polarization and the EIS method [7]. Results showed that the steel corrosion increases and corrosion current density increases with temperature in the range from 20 to 60 °C. The associated activation energy has been determined. Impedance curves showed that the charge transfer resistance (Rt) increases with increasing immersion duration. Parameters such as corrosion current density (Icorr), polarization resistance (Rp), and soil resistivity (ρ) can serve as the parameters for evaluation of soil corrosivity.

In [8], the electrochemical corrosion behavior of X70 pipeline steel in saline soil under capillary saline water was simulated to study the migration mechanism of saline solution on steel corrosion. The clay–silty loam type soil was taken near the buried gas pipelines. The results of the electrochemical tests showed that the corrosion was strongly influenced by the rise of saline capillary water. The corrosion current density and corrosion rate of X70 steel specimens increased with increasing NaCl content.

The corrosion behavior of pipeline carbon steel X36 (CSX36) in selected soil solutions from different pipeline soil environments was investigated using various electrochemical techniques [9]. The steel corrosion rate in all soil solutions studied decreased with an increase in immersion period. The corrosion potential Ecorr moved to negative values, indicating that the corrosion process was under cathodic control. The Icorr and 1/Rp tended to increase with decreasing soil resistivity, showing a proportional relationship between current resistance and current density but an inversely proportional relationship with resistivity. The soil corrosivity revealed that some soils are very corrosive with low resistivity.

The authors of [10] gave a method to evaluate corrosion in buried steel structures by estimating their lifespan based on non-electrochemical quantitative methods to estimate the corrosion rate by weight loss method. The technique consists of placing a metal specimen or a structure in different underground environments for a fixed period while considering their resistivity characteristics and soil composition. For resistivity < 500 $\Omega \cdot$cm, the soil is very corrosive. In addition, it has been shown that the severity of corrosion is the result of the combination of a large number of factors.

Probabilistic and statistical modeling methods have been used to assess the integrity of corroded pipelines. Statistical modeling methods used to estimate remaining pipeline life have focused on three main aspects: applications to estimate defect depth and corrosion rates, Bayesian applications in pipeline integrity to update the probability distribution of corrosion defects: depth, length and spatial dimension, distribution and pipeline reliability estimates [11]. Both stochastic models and distributions fitted from observed data can be used to estimate the reliability of oil and gas pipelines. The Monte Carlo simulation approach was used to forecast the long-term distribution of the pitting corrosion rate and pipeline reliability estimation. Bayesian data analysis provides a useful tool for the estimation of the probability distributions of the corrosion defect depth, length, and density.

The service life of the pipeline is affected by local corrosion failure due to liquid accumulation in the low-lying section of the buried natural gas pipeline causing external corrosion occurring at the interface between the pipeline and the soil [12]. Based on the Mises-Stress yield criterion, non-linear analysis was carried out with the finite element method (FEM). The effects of internal pressure, corrosion pit defect size, internal and external wall corrosion, corrosion pit group, and different types of volumetric corrosion pit defects on the failure of L360QS steel pipe were analyzed with consideration of the effects of corrosion pit axial and circumferential zones. The results provide a reference for failure

analysis and strength evaluation of buried L360QS steel pipe with corrosion defect. Pitting corrosion in offshore pipelines is the most prevalent type of external corrosion.

Study [13] explored the potential of deep learning models to predict the maximum depth of pitting corrosion in oil and gas pipelines. The models were trained considering various characteristics of the soil, where the pipe is buried, and different types of protective coatings of the pipes. Results demonstrate that deep learning models outperform all empirical and hybrid models applied in previous studies on the same dataset. The proposed model in the study has the potential to predict failure rates of the pipelines due to external corrosion and enhance the safety and reliability of these facilities.

The detection and characterization of surface steel defects such as corrosion defects, cracking, etc., as well as locating them identifying and determining their size and type is the phase to consider in order to define the maintenance methods. According to studies [14–26], steel surface defects have been detected and determined using non-destructive methods such as ultrasonic methods, which provide very precise real-time information on the position and size of the detected defect [14]. It can be used in line using the ultrasonic intelligent tool as an autonomous machine containing several ultrasonic probes to check the hydrocarbon transport pipeline [15]. The detection of material defects can be also carried out in an acoustic laboratory using specimens containing some artificially created defects [16]. It is based on the transmission and reflection of ultrasound waves within a material. The ultrasonic wave is emitted by a transducer placed on the surface of the material to be tested and propagates in the material by contact or immersion.

In the C-scan ultrasonic emission method [17], the acoustic energy is transferred to the component, dipping it completely into a water tank together with the transducers in order to locate defects and to determine their size. C-scan uses a projection of the ultrasonic data onto a plan view of the component being tested to create an image. This mapping technique is usually utilized for corrosion and other defects. The high-frequency ultrasonic C-scan is a technique to examine defect depth inside the material. The ultrasonic wave propagation uses standard tank immersion. A very high-frequency signal up to 50 MHz is transmitted to the sample by a focused transducer. The sample and the transducer are submerged in water that serves as the coupling medium. The initial signal is partially reflected back to the transducer at interfaces, defects, porosities, and at strong differences in acoustic impedance in the sample and the rest of the signal, if not fully reflected, continues through the sample. C-scan detection is very fast, precise, and repeatable. The detection is performed in real time even if a more in-depth analysis would be necessary to characterize the defects.

The time of flight diffraction technique (TOFD) ultrasonic technique [18] is mainly based on the analysis of the time of flight of the diffraction signals, which occur when an ultrasonic beam encounters an obstacle and re-emits omnidirectional waves by using the diffraction of the ultrasound beam caused by the presence of a discontinuity in the ultrasound path in order to locate surface defects and to determine their size. The method requires surface preparation and the use of coupling medium (oil, gel, etc.) to guarantee a transmission of the ultrasonic beam and facilitate the transducer scanning. This technique is a very sensitive method for detecting heterogeneities of the material and provides a quantitative appreciation of the true height of defects evidence such as in carbon steels.

Steel pipeline defect detection by ultrasonic testing is limited where the signal can be contaminated with backscatter noise, which masks fault echoes in the measured signal [19]. Signal processing is necessary to improve the signal-to-noise ratio and extract the defect classification. This article presents an overview of ultrasound signal processing techniques with and without an intelligent classifier. The common defects in pipelines are corrosion, crack, and porosity. Signal processing with an intelligent classifier achieves high precision, faster detection, and good fault classification.

The recent advances in non-destructive methods and assessment of corrosion undercoating in carbon–steel pipelines were discussed by the authors of [20]. Corrosion detection has led to the development of various sensors and monitoring methods based on various

non-destructive techniques. According to the authors' discussion, the acoustic method is better in terms of monitoring corrosion growth, localization, detection of micro-changes, and corrosion depth at a range of 2 m to 120 m. Data containing frequency information ranging from 0.1 to 1 MHz are processed using Fourier transform to divide the acoustic signal into frequency information. Corrosion prediction models and reliability assessment of carbon steel pipelines are used to predict the lifespan of structures. Future prospects are focused on creating various systems for detection, categorization, reliability prediction, and corrosion prevention.

The authors of one investigation studied the influence of material hardness and surface roughness on the result of longitudinal ultrasonic wave tests [21]. The samples had varying roughness from 0.34 to 250.73 μm and hardness from 32 to 57 HRC. The results showed that the speed of ultrasonic waves propagating in the material is influenced by the hardness of the material. It increases with high hardness, i.e., 57 HRC for longitudinal ultrasound. The absorption of the ultrasonic wave, estimated by the reduction in the gain of the successive reflection pulses of this wave, is imaged on the screen of an industrial or laboratory device. It is influenced both by the microstructure of the tested material estimated by its hardness and the surface roughness. A hard microstructure of martensitic steel with residual austenite showed a higher ultrasonic wave speed. The authors studied the problems of corrosion, detection, and monitoring of API 5L X60 steels for pipelines in petroleum products transmission [22]. The estimation of steel corrosion by soils was carried out by the weight loss method using corrosion coupons. Detection and corrosion monitoring of corrosion rate and metal loss was carried out by measuring the change in electrical resistance of steel exposed to the corrosive soil environment using an electrical resistance probe [23]. The instrument collects periodic data from sites by measuring the effects of electrochemical and mechanical corrosion components such as cavitations. The instrument produces a linearized signal proportional to the metal loss of the exposed element, which is a function of the thickness and geometry of the element to be analyzed. The reduction (metal loss) in the cross-section of the element due to corrosion is accompanied by a proportional increase in the electrical resistance of the element.

Defect material such as cracks has been characterized by estimating their size, dimension, and location using the ultrasonic TOFD method [24]. The ultrasonic testing technique is based on determination of the flight time of the diffracted echoes of the defect edges (diffraction time TOFD). To improve the arrival time of a TOFD signal, an estimation technique based on particle swarm optimization (PSO) and matching pursuit decomposition (MP) is proposed. The TOFD technique was modeled in a two-dimensional geometry using a software package. Simulation and experimental results proved the effectiveness of the proposed method.

The ultrasonic immersion testing method was used by the authors [25] to detect internal defects in a moving steel strip. The tested steel strip is immersed in water. An array of transmitting probes and an array of receiving probes span the width of the band such that the test covers the entire volume of the band. Inclusions can be detected at a signal-to-noise ratio between 9 and 10 dB. As a result, steel coils are maintained at a high level of internal cleanliness with a reduction in defects during the process.

Metallic material ultrasound detection using specimens including some artificially created defects was exposed to ultrasonic waves to establish a hypothetical appearance of natural defects [26]. The main objective is the detection of defects in metal samples by comparing simulated and experimental results. It turned out that there was a good correlation between the two methods, making it possible to use ultrasonic simulation as a detection method. The main objective of ultrasonic non-destructive testing is the detection of defects in metallic materials with respect to their primary data, i.e., size, shape, and position. The signal reflected in the material is compared to the signals obtained at a specific defect with those of the defect-free material. In this way, it is possible to determine the existence or absence of heterogeneities attributable to a specific defect.

More ultrasonic applications are in line with onshore or offshore inspection, such as hydrocarbon transport pipelines integrity using the ultrasonic intelligent tool or ultrasonic pig [27]. It is an intelligent industrial robotics technique where the data acquisition and processing tools are automatic and autonomous with a high level of detection. The machine contains several ultrasound probes evenly distributed to check the thickness of the entire circumference of the tube. External surface defects monitoring of GZ1 40" line was carried out by intelligent ultrasonic tool type "Magne Scan HR" [28]. The corrosion defects accounted for more than 93.6% of all identified defects.

The research design in this manuscript was prompted by soil corrosion problems encountered in buried gas transmission by steel pipeline lines where corrosion represents the main threat. The study was carried out by simulating aggressive soil using an artificial soil solution chemically reconstituted chosen as the most corrosive soil composition in order to understand the mechanisms and propose solutions. API5L X60 steel corrosion phenomenon resulting from electrochemical interaction with soil after protection failure has been studied in laboratory by simulating the industrial context. The study will consider the influence of some influencing parameters such as soil characteristics, pH, temperature, water content, and mechanical stresses. Electrochemical techniques will be employed to determine electrochemical parameters. The aim of this investigation is to better understand the corrosion phenomena of bare steel interaction with the soil. The second part of the investigation is to find solutions to the problems of detecting the surface anomalies caused by corrosion using non-destructive methods such as ultrasound and to demonstrate the applicability and effectiveness of the surface defects detection by non-destructive ultrasonic methods. We will use the C-scan ultrasonic emission method and the TOFD ultrasonic testing method to locate steel surface defects such as pitting corrosion and to determine their size and location using steel samples containing some artificial surface defects that have been analyzed in acoustics laboratory. The aim of this investigation part is to confirm the rapid and precise detection of the ultrasonic method, which provides suitable repair methods and adequate anti-corrosion solutions to enable rapid service resumption.

2. Materials and Methods

Steel samples were taken from the line after around thirty years of service and examined by ultrasounds using the intelligent tool showing some surface defects. The cutting process was chosen in order not to alter the microstructure and characteristics with the absence of heat and mechanical damage, due to its low heat input and the mechanical damage by avoiding the zones affected thermally. The samples were machined according to the required dimensions. The working electrode for electrochemical measurements is $(1.8 \times 1.0$ cm). The tensile test samples are of standardized size. The samples for the acoustic tests are $3 \times (10 \times 20$ cm), one of which includes a type V weld that will comprise some surface-created defects such as corrosion pits and weld defect. The samples underwent testing using C-scan ultrasonic emission tests and TOFD ultrasonic testing, and both immersion and non-immersion identify surface defects following acetone degreasing and mechanical polishing.

### 2.1. Steel Characterization

2.1.1. Steel Composition

The chemical composition of steel was determined through the spectrophotometric analysis on a "spectroRp 212" type machine (Table 1). The measured values were compared to the API standard values [2]. The results confirm as a manganese microalloy steel. A low carbon content ensures good weldability and mechanical resistance. Presence of manganese was a favorable and vanadium for hardening.

Table 1. Chemical composition (%) of API 5L X60 steel carried out by spectrophotometric analysis.

C	Si	Mn	P	S	Cr	Mo
0.018	0.036	1.400	0.017	0.013	0.028	0
Ni	**Al**	**Cu**	**Ti**	**V**	**Sn**	**Fe**
0.018	0.049	0.032	0.005	0.0061	0.0031	≈97.880

2.1.2. Microstructure

The micrographic analysis of API steel surfaces was carried out by optical microscope and by scanning electron microscope (SEM), type HITACHI TM—1000 (HITACHI, Tokyo, Japan). The samples were previously prepared by polishing and chemical attack by Nital solution 2%. The metallographic examinations (Figure 1) revealed a fine microstructure of ferrito-pearlitic type with a predominance of ferrite with clusters of pearlite at the grain boundaries. Some inclusions were observed, showing the probable presence of manganese sulfides. The steel is high yield strength steel (HLE) type and carbon steel micro alloyed.
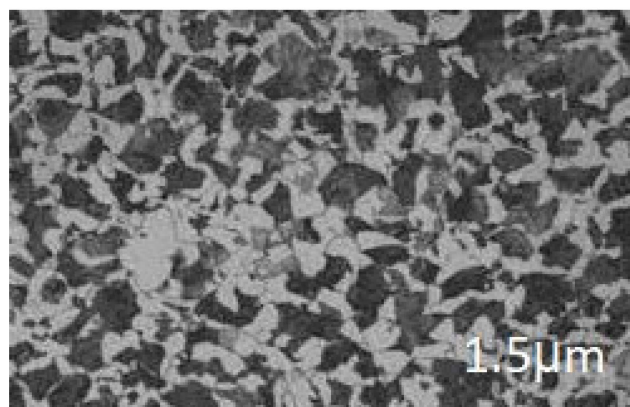
Figure 1. Microstructure of API 5L X60 pipeline steel after 30 s etch in 2% Nital solution.

2.1.3. Mechanical Characteristics

The mechanical characteristics of the API5L X60 steel according to the standard norm are reported in Table 2.

Table 2. Mechanical characteristics of API 5 L X60 steel according to the API standard norm.

	API Standard Values				
X60 Steel	**Re [MPa]**		**Rm [MPa]**		**A [%]**
	Min.	**Max.**	**Min.**	**Max.**	
	414	565	517	758	17.5–24

(Re: Elasticity limit, Rm: Rupture strength, A: Elongation at rupture).

The tensile test was carried out with and without the artificial simulated soil solution influence on flat specimens standardized according to the French standard (NF EN 100002-1 [1]) with a thickness of 9 mm taken from the tube previously machined according to the API 1104 standard [2]. The tests were carried out on a universal machine type CONTROLAB 30 with a maximum force of 600 KN. The test bench is equipped with force and elongation sensors. The machine is controlled by the "Universal Testing Machine" software (https://universal-motion.com/UniversalTestingSoftware.html), which follows the tensile curves at low speeds in order to provide information on the strength, rigidity and ductility of the analyzed steel.

The conventional characteristics were determined at room temperature (+25 °C) with and without the artificial simulated soil solution influence while exercising a deformation

until rupture, in order to determine the main mechanical characteristics such as the elasticity modulus, the Poisson's ratio, the elastic limit, the rupture strength, the elongation after rupture, and the coefficient of necking. The tensile tests were carried out on machined specimens having undergone before each test mechanical polishing and cleaning with acetone and air-dried after without immersion and immersion in the artificial simulated soil solution previously defined for immersion time from 7 to 90 days. The results are reported in Table 3.

Table 3. Mechanical characteristics of API 5L X60 flat specimens standardized steel after without immersion and immersion in the artificial simulated soil solution obtained by tensile tests at room temperature.

Test Number	Immersion Time		Re (MPa)	Rm (MPa)	A (%)	Z (%)
	(Days)	(h)				
1	-	-	570	664.222	20.0	23.905
2	7	168	500	623,916	20.0	55,517
3	28	672	480	599,939	18.4	57,361
4	60	1440	490	614,733	20.0	54,508
5	90	2160	510	652,995	20.0	59,722

(Z: striction).

2.2. Soil Solution

In order to determine the composition of the simulated soil solution for analysis, several soil samples have been taken from different specific locations of the line where corrosion defects have appeared and been analyzed by spectrophotometry microanalysis. Soil extract was prepared according to AFNOR French norm A–05.250 P.278. A mass of soil is taken then mixed with distilled water and analyzed by respecting the sampling procedures in order to eliminate any contamination or change in composition which may be caused by different parameters such as temperature or improper handling. The chemical composition of soil is given in Table 4 for the different sites Si considered [29]. We have chosen the most aggressive composition for analysis. The aggressiveness criterion chosen is mainly the content of elements favoring the interaction of the steel with the soil such as chloride, sulphate, and bicarbonate ions [4]. The artificial test solution for corrosion analysis called "soil simulating solution" is obtained by reconstitution of the chemical composition of the most aggressive soil composition, which has a significant corrosive character such as resistivity, conductivity, and pH (Table 5).

Table 4. Chemical composition of soil solutions taken from various GZ1 sites. (Si: number of the soil [29].

| S_i Sites	Mass of Soil (mg/L)					
	Ca^{2+}	Mg^{2+}	K^+	Cl^-	SO_4^{2-}	HCO_3^-
S_1	94.60	56	7.6	76.9	736	117
S_2	18.96	16.44	11.7	47.33	458.4	183
S_3	----	---	6	7.8	74	218
S_4	2.00	29.04	1.82	22.69	37.48	160

Table 5. Chemical composition of the reconstituted soil solution as the most aggressive soil solution called "artificial soil simulating solution" chosen for analysis.

| Component	$CaSO_4$	$MgSO_4$	K_2SO_4	NaCl	Na_2SO_4	$NaHCO_3$
concentration (g/L)	0.02	0.29	0.018	0.23	0.38	0.16

2.3. Corrosion Tests

The potentiodynamic polarization tests were carried out using a Potentiostat/Galvanostat Model 273 A, controlled by corrosion analysis software (Soft corr III). Measurements were obtained using a glass conventional three-electrode cell with a capacity of 500 mL including a graphite counter electrode and a saturated calomel electrode (SCE) as reference. The working electrode was machined with a section of 1.8 cm^2. The potentiodynamic current and potential were recorded by varying the potential from -1400 mV to -400 mV with a scanning rate of 1.68 mV/s. All tests were performed in de-aerated solutions under continuously stirred conditions at a constant temperature in the range of 25–50 $\pm$ 0.1 °C using a thermostat. A free potential corrosion test was carried out (Figure 2). It shows a potential stabilization at a value of approximately -734 mV after 15 min and a sudden decrease. The anodic and cathodic polarization parameters were studied as a function of the pH after 1 h of immersion, at a temperature of 25 °C $\pm$ 0.1, a pH varying from 4.0 to 8.0 at temperature 25 °C (Figure 3), and a temperature in the range 25 to 50 °C at pH 6.0 (Figure 4). The pH range was chosen by simulating the soil where the pH is between 4 and 10, predominantly acidic, containing some humified organic matter.
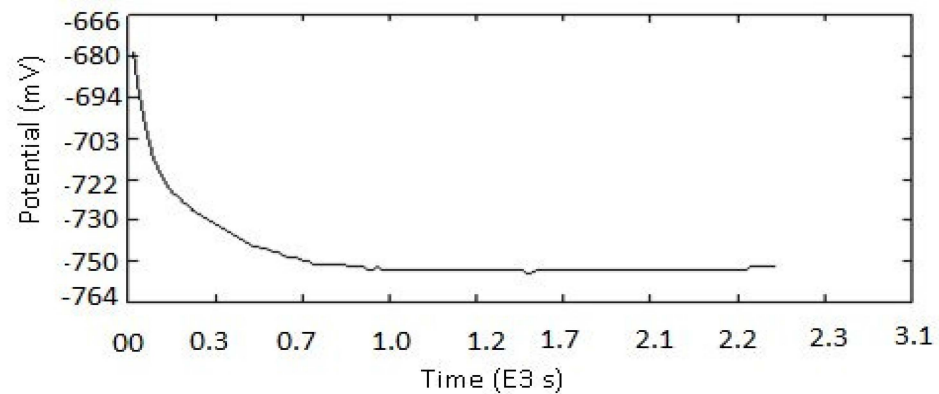
Figure 2. Evolution of the free potential corrosion as a function of time (t = f (E)) for API 5L X60 steel immersed in artificial soil simulating solution.
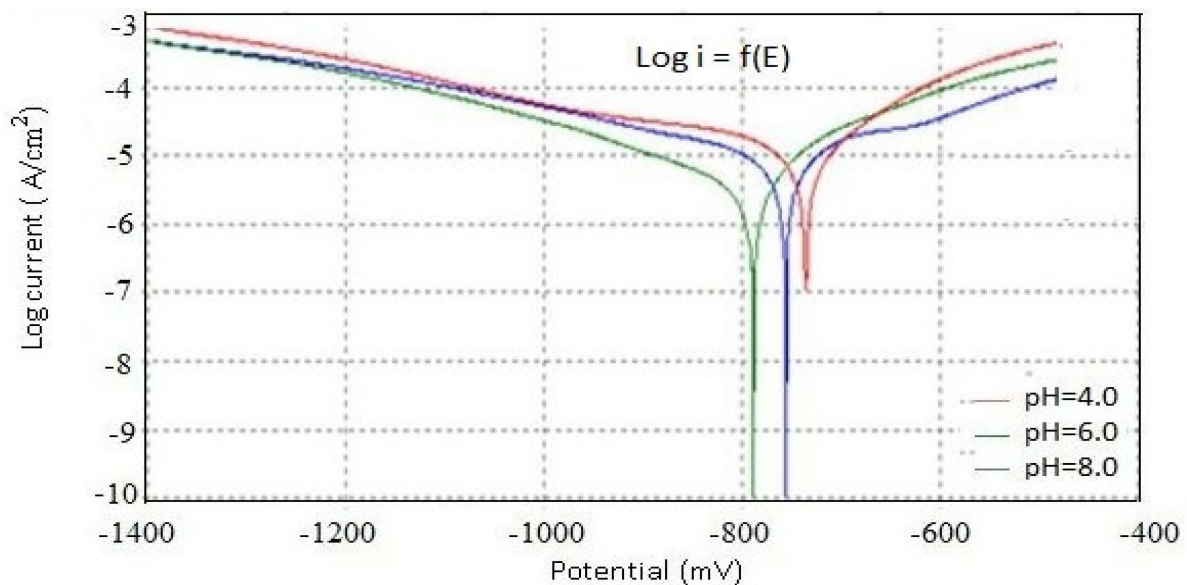
Figure 3. Potentiodynamic polarization curves (Log i = f (E) for API 5L X60 steel in artificial soil simulating solution at pH values in the range 4.0 to 8.0 and a temperature of 25 °C.
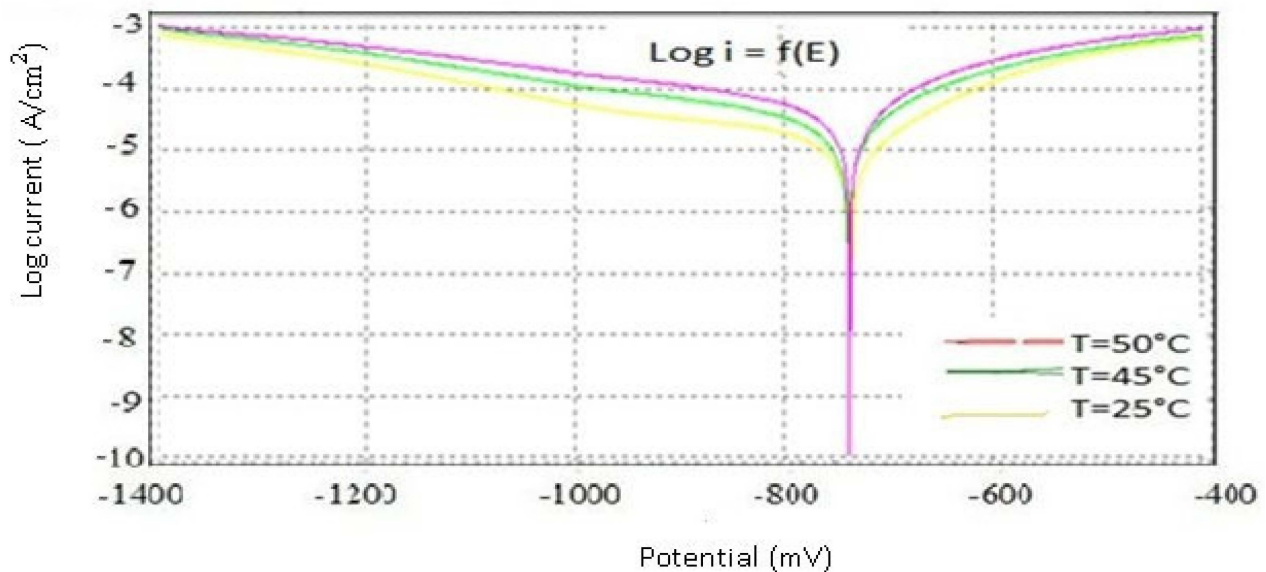
Figure 4. Potentiodynamic polarization curves (Log i = f (E) for API 5L X60 steel in artificial soil simulating solution at temperature range 25 to 50 °C and a pH = 6.0.

2.4. Ultrasonic Steel Tests

Steel samples containing some artificial surface defects such as a corrosion pits and welding defect were previously machined according to the required dimensions and immersed in the artificial soil solution. A preliminary treatment was carried out comprising a degreasing operation with acetone and distilled water in order to remove any traces of grease and foreign matter. The samples were dried in an air stream to avoid any reaction of water and mechanically polished by abrasive papers 600 and 1200. The samples after preparation were analyzed in the laboratory by non-destructive methods using the ultrasound technique by C-scan and TOFD. Steel samples' surfaces have been exposed to ultrasonic waves by varying the incidence angle in the range 45°, 60° or70°. Generating ultrasonic waves in the steel causes the propagation of coherent waves that propagate into the steel to detect different types of defects. Two transducers, one operating in transmission, other in reception, are placed equidistant on either side of the thickness. The beam from each of the two transducers must be sufficiently diverging to cover the complete thickness. The edges of the defects diffract the ultrasonic waves and generate defect echoes. Software allows the acquisition of the signals and their processing. For the determination of the measurements' accuracy, it is necessary to evaluate some parameters such as the propagation speed of ultrasound in carbon steel, the shape and position of the defects, the thickness to be checked, and the frequency and angle of incidence of the transducers. A scanner is needed to position the two probes on each side of the thickness and to install the encoder. The analysis is affected by means of two opposed ultrasonic transducers, one operating in transmission and the other in reception. The transducer is placed at equal distances on either side of the thickness to be examined, so as to cover the entire thickness of the part to be checked. The image obtained is a transverse representation of the thickness.

Ultrasonic tests were carried out using three types of steel samples: the first does not contain any surface defect, the second contains a surface defect in the form of a corrosion pit, and the third contains a corrosion pit with a welding defect. The ultrasound spectra and images are shown as following. The ultrasonic spectrum for the first sample not containing any surface defect was obtained by TOFD ultrasonic method on a steel plate (10 × 20 cm) subjected to diffracted ultrasonic waves. The analysis was carried out using two opposed ultrasonic transducers, one operating in transmission and the other in reception. The results are shown in Figure 5. The same first sample was analysed by the C-scan ultrasound method in order to examine the depth of the steel surface defects. The steel sample and

the transducer were immersed in the standard water tank, which serves as the coupling medium. A very high-frequency signal (up to 50 MHz) was transmitted to the sample by a transducer. The results are reported in Figure 6. The ultrasonic spectrum was obtained for the second steel sample (10 × 20 cm) containing surface defects in the form of corrosion pitting. The sample was subjected to an ultrasonic wave diffracted by the TOFD method and by ultrasonic immersion. The results are reported in Figures 7 and 8. The third sample contains surface defects in the form of corrosion pits and welding defects. They were characterized by the non-contact ultrasonic method and by ultrasonic immersion. The initial signal is reflected back to the transducer at the interfaces, defects, and strong acoustic impedance differences in the sample. The rest of the signal, if not fully reflected, continues through the sample. The TOFD ultrasonic spectra of the different samples showed a red colour corresponding to the appearance of the first peak of the considered defect while the green colour to the absence or the appearance of the next peak.
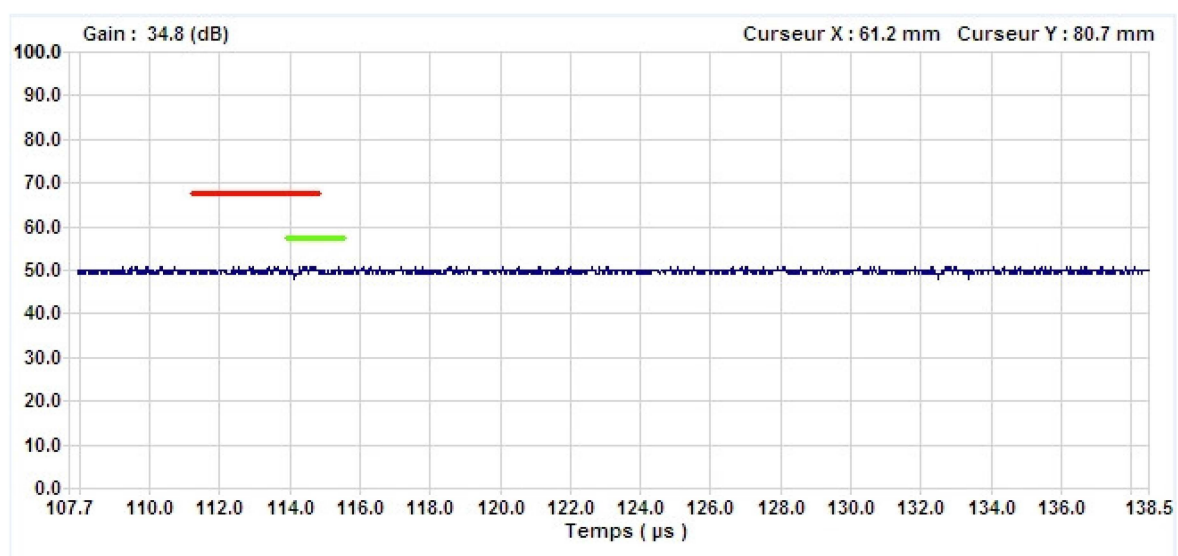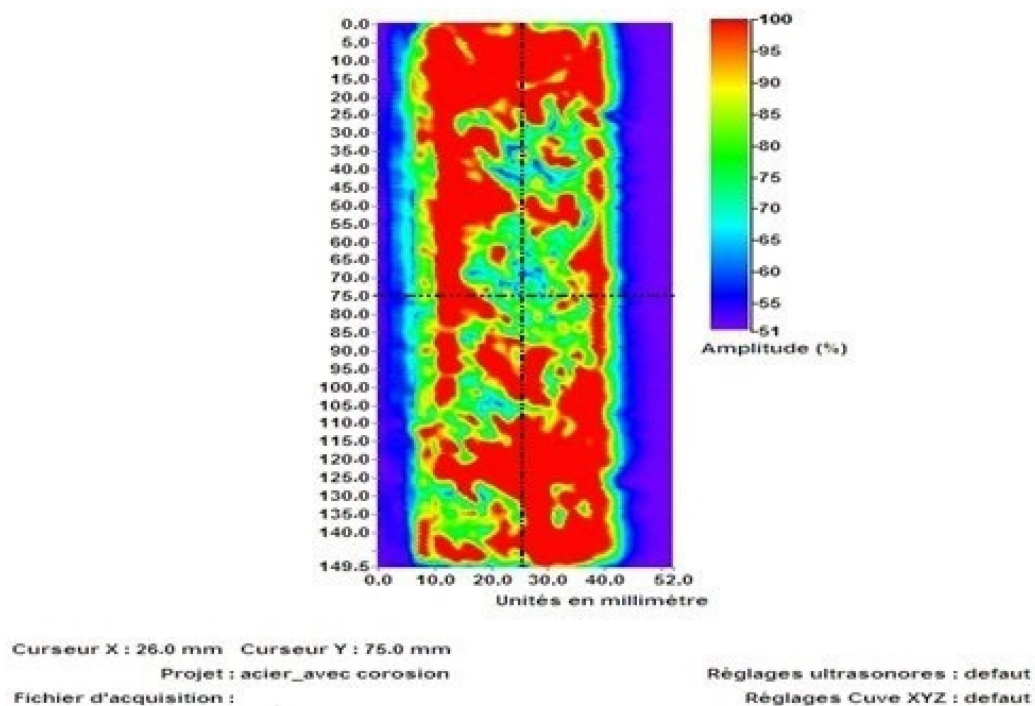

Figure 5. TOFD ultrasound spectrum of first steel sample (10 × 20 cm) not containing any surface defect. (Time (µs).)
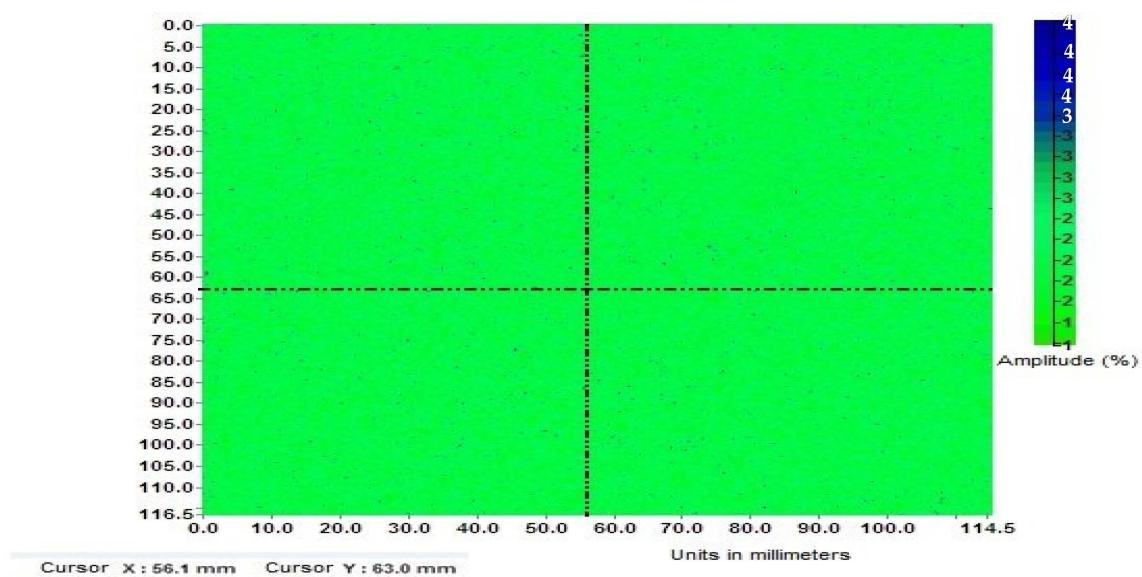
Figure 6. C-scan ultrasonic image of the first steel sample (10 × 10 cm) not containing any surface defect. (Amplitude (%)).
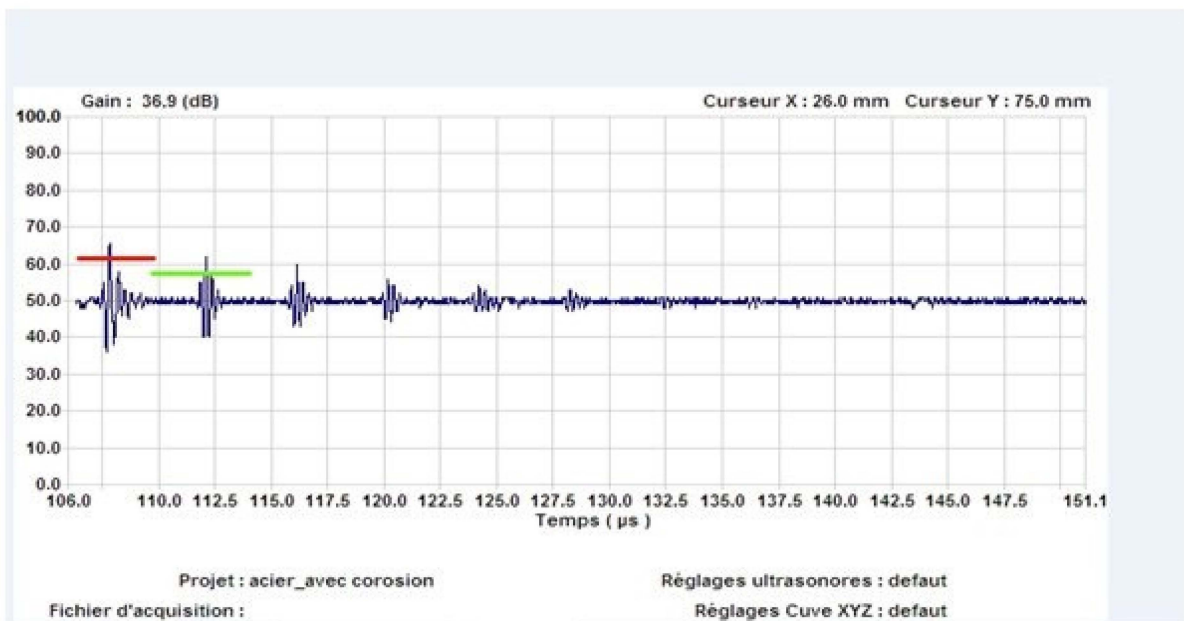
Figure 7. TOFD ultrasound spectrum of the second steel sample (10 × 20 cm) containing a surface defect in corrosion pit form (Time (µs)).

Figure 8. C-scan ultrasound image of the second steel sample (10 × 20 cm) containing a surface defect in corrosion pit form (Amplitude (%).)

3. Results and Discussions

Steel gas pipeline transport is a reliable means and meets environmental safety requirements. However, the steel is highly susceptible to damage by corrosive phenomena after exploitation due to chemical reactions with their soil environment, which often results in severe deterioration in the properties of the material both directly and indirectly. Steel gas pipeline inspections by an in line intelligent ultrasonic tool after several years of service showed numerous defects on the exterior walls and fewer on the interior walls, such as loss

of thickness, tube perforation, pitting corrosion, welding defects, cracking, etc. External corrosion defects are the majority among all identified defects in consequence of various electrochemical solicitations of the bare steel with the soil after protection failure by passive coating and active cathodic protection. Defaults risks resulting from the external chemical interaction are preoccupying phenomena in the oil industry and research laboratory. They are the major threats that can reduce the structural integrity of pipelines' transmission system, which requires knowledge of the corrosion mechanisms by soils, the influence of physical parameters, and the means of identifying and characterizing defects.

To study the carbon steel corrosion phenomenon in laboratory, we have used an artificial soil solution by approaching the industrial context using a chemically reconstituted solution as soil simulating solution chosen as the most corrosive soil composition among the soil compositions analyzed where the pipeline is buried and the steel damaged. Electrochemical parameters have been determined using electrochemical techniques by varying the physical parameters such as temperature, pH, and the mechanical stresses influence. The chemical composition of the steel and its microstructure were analyzed. To detect and identify the steel surface defects, we have used samples containing artificial corrosion pitting and welding defects by exposing to ultrasonic analysis methods (C-scan and TOFD) conventional non-destructive.

3.1. Steel Properties

The measured values of the chemical characteristics of X60 steel are carried out by spectrophotometric analysis as shown above. It is a micro-alloyed steel type with high elastic limit (HLE) and low carbon content ensuring good weldability and good resistance to corrosion and mechanical parameters. Manganese is the only favourable element that exists in the form of MnS, or carbide Mn_3C associated with cementite Fe_3C, that increases the steel hardness and hardenability and limits the harmful effect of sulfur in its combined form. High content of phosphorus in its combination with ferrite has an adverse effect by causing a grain coarsening, which increases the steel's cold brittleness while decreasing plasticity and ductility. Hence, the refining of the ferritic grain is performed to increase the steel's strength needed.

The chemical characteristics results have been compared to the standard values of the API norm [2]. These values showed that the steel conforms to the norm with adequate values in its composition.

The microstructure analysis showed that the X60 steel has a ferrite-pearlitic type microstructure with a predominance of refining ferritic with clusters of pearlite. Some inclusions were observed, showing the probable presence of manganese sulfides. The refinement of ferritic grain size obtained by different mechanisms of hardening and precipitation during steel manufacturing has the consequence to have a better resistance to corrosion.

The mechanical characteristics of the studied steel were determined at ambient temperature from the tensile specimens previously machined according to the required standardized test dimensions. The obtained values are reported in Table 3 of the main mechanical characteristics such as the elasticity modulus, the rupture strength, the elongation after breaking, and the coefficient of necking. The values were compared with the standard values. The steel conforms to the API norm. The mechanical characteristics were determined in order to consider the possible influence of corrosion, which may generate some surface defects by mechanical stress in addition to steel interaction with the soil after the exterior protection failure baring of the steel. Results (Table 3) showed that the mechanical characteristics values changed as a consequence of mechanical stresses and the interaction of the soil solution after immersion in the simulated soil solution for a duration of 168 h to 2160 h obtained by tensile tests at room temperature. The rupture strength gradually decreases over time from 664 MPa to 560 MPa after immersion of 672 h. This decrease is mainly due to the duration of specimen's exposure in soil solution, which is the cause of direct degradation of the mechanical characteristics of steel. After immersion for 2160 h, the rupture strength increases up to 653 Mpa but does not reach the initial value. This

increase is due to the formation of a protective layer of oxide on the surface, which protects the steel from corrosion and consequently from any degradation of the steel. The resistance time of this protective layer has not been determined because the tests were not continued beyond a 2160 h immersion time. This layer will eventually degrade, which will cause a ductile rupture even more fragile. The necking at rupture noted Z is expressed in %, which corresponds to the reduction in the section of the deformation zone by necking during the rupture. The necking initially had a value of 23.91% after progressive immersion in the soil solution for variable durations. The necking values are relatively stable, which explains that the duration of a specimen's exposure in the simulated soil solution did not have a great influence on the elongation and the values of the deformation by necking. Mechanical characteristics results show that the corrosion process can be accentuated when the steel in addition to its interactions with the soil solution is solicited by mechanical stresses. Stress corrosion can occur near pitting potential or near passivation potential, explaining the minimum time to failure. The potential regions favourable to stress corrosion have the common characteristics that the passive film has only a reduced stability and the metal can easily turn from the active state to the passive state and vice versa.

3.2. Steel Corrosion

X60 steel corrosion was carried out in aggressive artificial soil solution reconstituted from chemical analyses of soils taken from various sites (Table 4). The current–potential curves were recorded by varying the potential. The anodic and cathodic polarization parameters were studied as a function of the pH and temperature, as shown in Figures 3 and 4. Steel corrosion at free potential in Figure 2 shows an early high potential evolution towards more negative values, which indicates that corrosion reactions take place on the metallic surface and the interface state (electrode/electrolyte) is modified. A stabilization of the potential at a value of approximately -734 mV was obtained after a sudden decrease, which corresponds to the value of the corrosion potential (Ecorr) or mixed corrosion of the steel in the soil simulating solution and a thermodynamic equilibrium state where the oxidizing/reducing systems, which participate in the corrosion, have the same kinetics throughout the immersion.

The corrosion of steel is a function of pH, as shown in the results of the polarization curves. If the pH values decrease towards neutral or acidic pH in the range of 4.0 to 8.0, the corrosion of the steel increases, the resistance polarization decreases, and the corrosion potential tends towards anodic values. The pH results are quite the opposite when the environment is basic (pH = 8.0); steel corrosion decreases and polarization resistance increases. A de-aerated simulating soil solution has been used under continuously stirred conditions at constant temperature and bubbling with nitrogen in order to deoxygenate the solution and avoid any corrosion due to the effect of pH and oxygen reactions, which promotes the corrosion rate. Some studies in the literature have shown that when steel is exposed to moist aerated soils containing dissolved oxygen, the rate of corrosion will depend on the rate at which the oxygen reacts with the absorbed atomic hydrogen, thus depolarizing the surface and allowing the reduction reaction to continue.

In the temperature range of 25 °C to 50 °C, as shown in the results of the polarization curves, the steel corrosion is a function of temperature. The corrosion current density increases with increasing temperature. The corrosion potential of the immersed steel in the simulated soil solution shifts towards negative values as the temperature increases. The anodic polarization curves present straight parallel Tafel lines, indicating that the hydrogen reduction reaction on the steel surface to be studied is still present according to the activation mechanism in the temperature range. The corrosion activation energy increases with temperature on the simulated soil solution. These values are close to those in the literature. The variations of the electrochemical parameters under the effect of the temperature in the studied range 25–50 °C for a pH near neutral confirm the effect of the temperature on the corrosion of steel in the real soil as a result of the variation of the seasonal temperature where the difference is significant. This can modify the electrochemical interactions of the steel with the surrounding soil environment.

Corrosion results from simulated artificial soil solutions showed that the steel tubes of gas pipelines are sensitive to corrosion when protection is failing. The corrosion phenomenon is accentuated by some parameters such as soil characteristics, pH, soil composition, resistivity, water content, as well mechanical stresses. According to the literature [30], the refinement of the steel grain improves resistance to corrosion.

3.3. Ultrasonic Steel Detection

The ultrasonic propagation in massive solids is the existence of two modes of vibration (longitudinal and transverse), which propagate at different speeds. In the longitudinal mode, the metal atoms vibrate parallel to the direction of propagation, where in the transverse mode, the vibration is perpendicular to the propagation. In steel material, the speed of the longitudinal waves is 5940 m·s^{-1} and the speed of the transverse waves is 3265 m·s^{-1} for steel not containing any defects. The speed of wave propagation depends on the steel material characteristic parameters like the elasticity longitudinal modulus, the density, and the friction coefficient [31].

Steel samples containing some artificial surface defects such as a corrosion pits and welding defect were analyzed in the laboratory by ultrasound non-destructive methods using the ultrasonic method by a diffracted ultrasonic wave and immersion. The analysis was carried out using two opposed ultrasonic transducers, one operating in transmission, the other in reception, placed equidistant on either side of the thickness. The edges of the defects diffract the ultrasonic waves and generate defect echoes. They also were analysed by the immersion ultrasound method in order to examine the depth of the steel surface defects. The steel sample and the transducer were immersed in the standard water tank, which serves as the coupling medium. A very high-frequency signal (up to 50 MHz) was transmitted to the sample by a transducer. The samples' surfaces have been exposed to ultrasonic waves by varying the incidence angle in the range 45°, 60° or 70°. Generating ultrasonic waves in the steel causes the propagation of coherent waves that propagate into the steel to detect different types of defects. Software allows the acquisition of the signals and their processing.

Ultrasonic spectra were carried out on three types of steel samples; the first does not contains any surface defect, the second contains a surface defect in the form of a corrosion pit, and the third contains a corrosion pit with a welding defect. The first steel sample not containing any surface defect characterized by the non-contact ultrasonic method and by ultrasonic immersion showed that the diffracted ultrasonic wave occurring at the edges of the defects does not appear (Figure 5). The initial signal was not reflected towards the transducer, resulting in the defect's absence. The signal remains stable in all instants from 0 to 138.2 µs at a maximum amplitude of 50 dB. The C-scan ultrasonic image obtained by the mapping technique after projecting of the ultrasonic data into a plan view of the steel sample where not containing any surface defect (Figure 6) presents a single reflection that does not change even when the amplitude of cursors x and y vary. The image is partially clear, with a unique distribution even for a variation of the amplitude of the cursors which clearly shows the absence of surface defects. These results indicate that the first steel sample not containing defect presents an image by simple reflection of the ultrasonic beam on interfaces having the same acoustic impedances.

The second steel sample containing surface defects in the form of corrosion pitting analyzed by the non-contact ultrasonic method and ultrasonic immersion showed the ultrasonic spectrum reported in Figures 7 and 8. After propagation of the ultrasonic waves, the diffracted ultrasonic reflected wave occurring at the edges of the defects appears due to the presence of a corrosion defect. The analysis of the time of flight of the diffraction signals when an ultrasonic beam encounters an obstacle such as corrosion pits re-emits omnidirectional waves. TOFD ultrasound spectra (Figure 7) show at a time of 108.2 µs and a maximum amplitude of about 62 dB, but the signal was still considerable at 112.5 µs and 115.3 µs and the signal amplitude was almost equal to the noise level. C-scan ultrasonic image of the steel sample containing corrosion pits surface defect (Figure 8) presents a distribution resulting from surface reflection including corrosion defect after variation of the amplitude of cursors x and y. These results indicate that

the second steel sample containing defect presents an image by reflection of the ultrasonic beam on interfaces having different acoustic impedances. The results showed also that the presence of corrosion pits defaults on the surface steel has modified the propagation of transverse ultrasonic waves through the steel, showing a slight increase of 3437.5 m·s^{-1} according to Equation (2) compared to the theoretical speed of wave propagation in steel without defects of 3265 m· s^{-1}. The cross-transverse speed ultrasonic propagation through the plate including corrosion defect is:

$$V_T = \frac{2d}{\Delta T} \tag{1}$$

where V_T: transverse speed—$2d$: crossed distance by the wave—ΔT: emission and reflection time.

$$V_T = \frac{110}{3.2} = 34.375 \text{ μs} = 3437.5 \text{ m/s} \tag{2}$$

The third sample contains surface defects in the form of corrosion pits and welding defects. They were characterized by the non-contact ultrasonic method and by ultrasonic immersion (Figures 9–11). The initial signal is reflected back to the transducer at the interfaces, defects, and acoustic impedance differences in the sample. After the ultrasonic waves propagate on the welded sample with corrosion, the diffracted ultrasonic wave occurs at the edges of the defects; this indicates that welded defects are confined to the center of the plate, and we note the spread of the corrosion on most of the plate with time. The first defect represents the weld defect at the edge of the plate. TOFD ultrasound spectra (Figure 9) show at a time of 123.1 μs maximum amplitude of about 93 dB. All typical welding defects are detected. There are small gaps at the weld level that increase in size over time due to the second corrosion defect detected. C-scan ultrasonic image of the steel sample containing corrosion pits and weld (Figures 10 and 11) presents a different distribution resulting from these defects and a different variation of the amplitude. These results indicate that the third steel sample containing defect presents an image by reflection of the ultrasonic beam on interfaces having different acoustic impedances. The results showed also that the presence of defaults on the surface steel has modified the propagation of transverse ultrasonic waves through the steel, showing a high increase of 4621.21 m·s^{-1} according to Equation (3) compared to the theoretical speed in steel without defects.

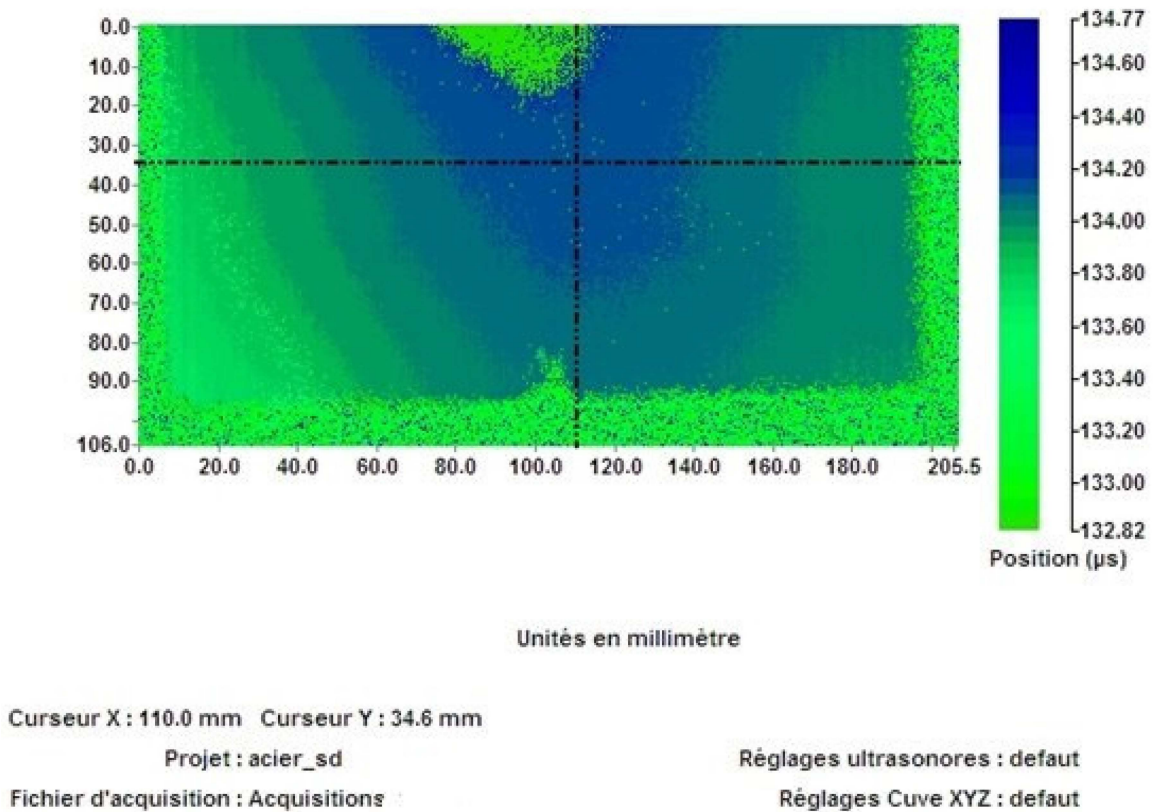$$V_T = \frac{122}{2.64} = 46.2121 \text{ μs} = 4621.21 \text{ m/s} \tag{3}$$
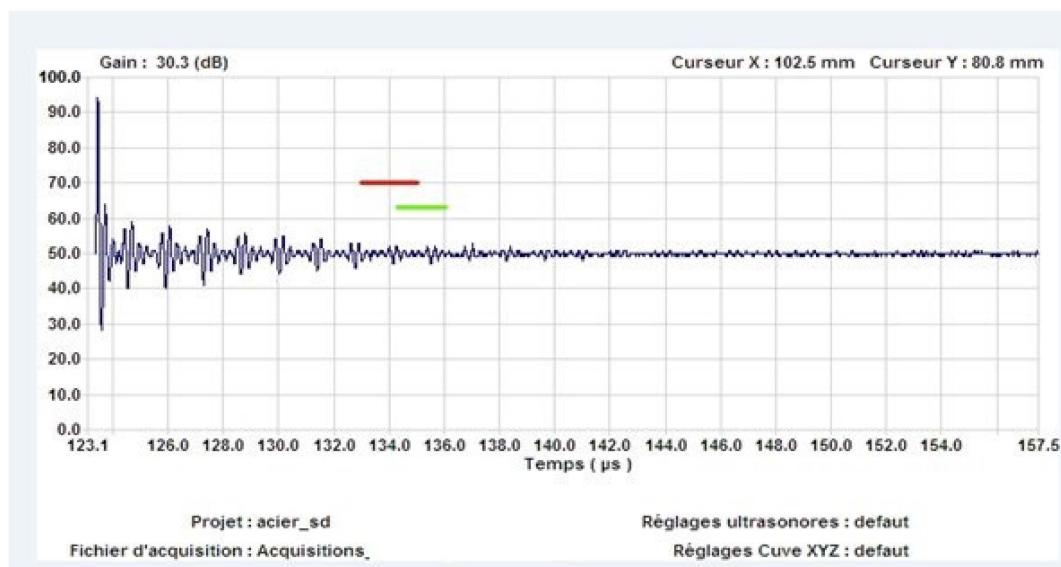
Figure 9. TOFD ultrasound spectrum of the third steel sample (10 × 20 cm) containing more surface defects as corrosion pits and welded defect (Time (μs)).
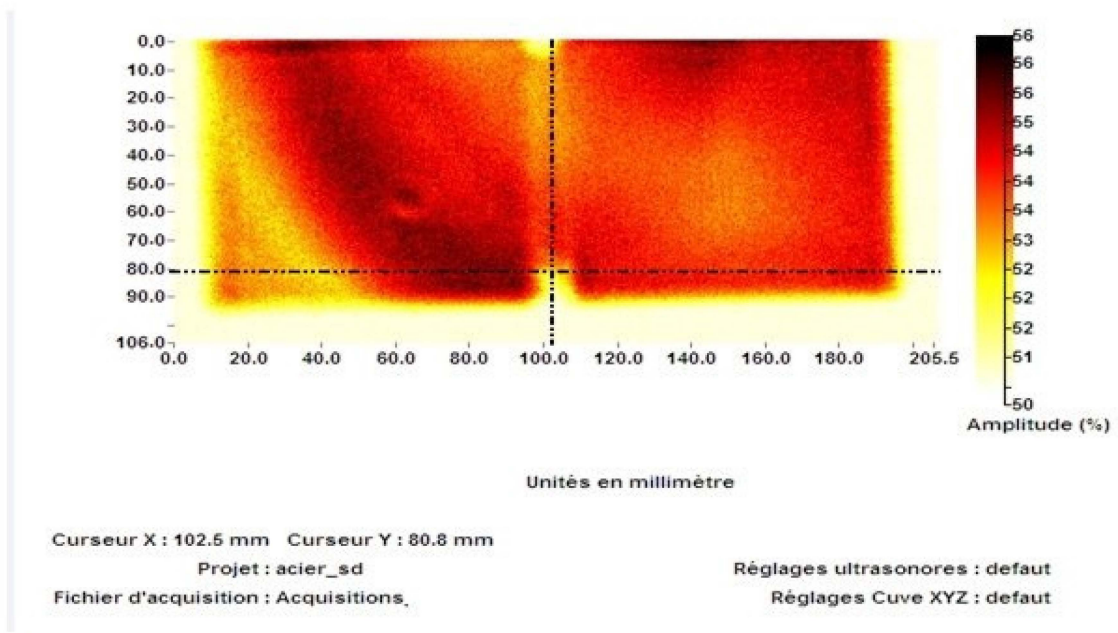
Figure 10. C-scan ultrasound image of the third steel sample (10 × 20 cm) containing more surface defects as corrosion pits and welded defect (Amplitude (%)).

Figure 11. C-scan ultrasound image of the third steel sample (10 × 20 cm) containing more surface defects as corrosion pits and welded defect (Position (μs)).

Surface defects increase, and the cross-transverse speed of ultrasonic propagation through the plate including defect increases.

4. Conclusions

In this manuscript, the X60 steel corrosion phenomenon has been studied by using an artificial soil solution chemically reconstituted chosen as the most corrosive soil composition. C-scan and TOFD ultrasonic testing methods where used to detect and characterize steel surface defects. The following conclusions were obtained:

➢ Steel chemical composition and mechanical characteristics results conform to the API norms for steel.

➢ Microstructure is a ferrite-pearlitic type with a predominance of refining ferritic grain with clusters of pearlite.

➢ Steel is sensitive to corrosion by soil when protection is failing. It is accentuated by some parameters such as soil characteristics, pH, soil composition, resistivity, water content, as well mechanical stresses.

➢ The diffracted ultrasonic wave occurring at the edges of the defects does not appear for steel not containing any defect. The initial signal was not reflected towards the transducer, which remains stable in all instants. The ultrasonic image presents a single reflection, which does not change by amplitude variation. The ultrasonic beam on interfaces has the same acoustic impedances.

➢ The diffracted ultrasonic reflected wave occurring at the edges of the corrosion pit defects appears due to the presence of a defect ultrasonic image, which presents a distribution resulting from surface reflection including corrosion defect after variation of the amplitude. The ultrasonic beam on interfaces has different acoustic impedances.

➢ The speed propagation of transverse ultrasonic waves through the steel is modified, showing a slight increase compared to the theoretical speed of wave propagation in steel without defects.

➢ The diffracted ultrasonic wave occurs at the edges of the defected steel in the form of corrosion pits and welding defects, which indicated that welded defect a are confined to the center of the plate. The first defect represents the weld defect. There are small gaps at the weld level, which increase in size over time due to the second corrosion defects detected. Ultrasonic image presents a distribution resulting from different variations of the amplitude and different acoustic impedances.

➢ The cross-transverse speed ultrasonic propagation through the plate including corrosion pits and weld defect is modified, showing a high increase.

➢ Ultrasonic method can be used in the industrial context as an intelligent industrial robotics technique where the data acquisition and processing tools are automatic and autonomous with a high level of detection. The maintenance strategy can be adopted as a preventive form to plan regular inline inspections to detect defect nature, location, and sizing.

➢ Future studies should aim to better understand the corrosion phenomena to develop some advanced non-destructive testing methods and corrosion inhibitor protection from natural sources, economical, and practical methods using new ecological, biodegradable, and non-toxic formulations according to the concept of sustainable development [32,33].

Author Contributions: Conceptualization, A.B.; methodology, A.B.; software, S.A.B.; validation, A.B. and I.B.; formal analysis, A.B.; investigation, F.B., A.A.Z. and S.A.B.; resources, I.B.; data curation, F.B., A.A.Z. and S.A.B.; writing—original draft preparation, F.B.; writing—review and editing, A.B.; visualization, I.B.; supervision, A.B.; project administration, I.B. All authors have read and agreed to the published version of the manuscript.

Data Availability Statement: The data presented in this study are available on request from the corresponding author. The data are not publicly available due to current research by future doctoral students.

References

1. Benmousa, A.; Hadjel, M.; Traisnel, M. Corrosion behavior of API 5LX-60 pipeline steel exposed to near-neutral pH soil simulating solution. *Mater. Corros.* **2006**, *57*, 771–777. [CrossRef]
2. *API Specification 5L (SPEC 5L), Specification for Line Pipe*, 14th ed.; American Petroleum Institute: Washington, DC, USA, 46th Edition Updated on 2023. Available online: https://www.octalsteel.com/api-5l-pipe-specification/#:~:text=API%205L%20Pipe%20Specification%20(46th%20Edition%20Updated%20on%202023)&text=API%205L%20pipes%20are%20carbon,onshore,%20offshore%20and%20sour%20services (accessed on 18 March 2024).
3. Akkouche, R.; Rémazeilles, C.; Jeannin, M.; Barbalat, M.; Sabot, R.; Refait, P. Influence of soil moisture on the corrosion processes of carbon steel in artificial soil: Active area and aeration cells. *Electrochim. Acta* **2016**, *213*, 698–708. [CrossRef]
4. Benmoussat, A.; Hadjel, M. Corrosion behaviour of low carbon line pipe in soil environment. *J. Corros. Sci. Eng.* **2005**, *7*, 147156.
5. Pérez, T.; Domínguez-Aguilar, M.A.; Alamilla, J.L.; Liu, H.; Contreras, A.; Ake, L.M.Q. Corrosion behavior of low carbon steels anf non-ferrous metals exposed to a real calcarepous soil environment. *De Gruyer* **2022**. [CrossRef]
6. Bai, X.; He, B.; Han, P.; Xie, R.; Sun, F.; Chen, Z.; Wang, Y.; Liu, X. Corrosion behavior and mechanism of X80 steel in silty soil under the combined effect of salt and temperature. *RSC Adv.* **2021**, *12*, 129–147. [CrossRef]
7. Benmoussat, A.; Hadjiat, H.; Hadjel, M. External Damage by Corrosion on Steel Gas Pipeline. *Eurasian ChemTech J.* **2001**, *3*, 285–289. [CrossRef]
8. Wei, J.; He, B.; Feng, Y.; Hou, L.; Han, P.; Bai, X. Electrochemical Corrosion Behaviour of X70 Steel under the Action of Capillary Water in Saline Soils. *Materials* **2022**, *15*, 3426. [CrossRef]
9. Noor, E.A.; Al-Moubaraki, A.H.; Al-Masoudi, D.I.; Chafiq, M.; Chaouiki, A.; Ko, Y.G. Corrosion Behavior of Carbon Steel X36 in Solutions of Soils Collected from Different Areas Linked to the Main Pipe Network of a Water Distribution System in Jeddah City. *Metals* **2023**, *13*, 670. [CrossRef]
10. Arriba-Rodriguez, L.-D.; Villanueva-Balsera, J.; Ortega-Fernandez, F.; Rodriguez-Perez, F. Methods to Evaluate Corrosion in Buried Steel Structures: A Review. *Metals* **2018**, *8*, 334. [CrossRef]
11. Velázquez, J.C.; Hernández-Sánchez, E.; Terán, G.; Capula-Colindres, S.; Diaz-Cruz, M.; Cervantes-Tobón, A. Probabilistic and Statistical Techniques to Study the Impact of Localized Corrosion Defects in Oil and Gas Pipelines: A Review. *Metals* **2022**, *12*, 576. [CrossRef]
12. Zhang, J.; Lian, Z.; Zhou, Z.; Song, Z.; Liu, M.; Yang, K.; Liu, Z. Safety and reliability assessment of external corrosion defects assessment of buried pipelines—Soil interface: A mechanisms and finite element study. *J. Loss Prev. Process Ind.* **2023**, *82*, 105006. [CrossRef]
13. Akhlaghi, B.; Mesghali, H.; Ehteshami, M.; Mohammadpour, J.; Salehi, F.; Abbassi, R. Predictive deep learning for pitting corrosion modeling in buried transmission pipelines. *Process. Saf. Environ. Prot.* **2023**, *174*, 320–327. [CrossRef]
14. Krautkrämer, J.; Krautkrämer, H. *Ultrasonic Testing of Materials*, 3rd ed.; Springer: Berlin/Heidelberg, Germany, 1983.
15. Amsellem, C.; Edery, R.; Scanu, M.; Martin, L. Contrôle de Pipelines et de Canalisations Par Racleursinstrumentés Par Ultrasons. In Proceedings of the Cofrend 2011, National NDT Seminar & Exhibition, Dunkerque, France, 24–27 May 2011; Available online: https://www.ndt.net/?id=12051 (accessed on 18 March 2024).
16. Gunn, D.A.; Holyoake, S.J.; Dashwood, B.A.; Wilkinson, P.B.; Brett, C.R.; Wallis, H.C.; Leman, W.; Rees, J.G. Ultrasonic Testing of Laboratory Samples Representing Monopile Wind Turbine Foundations. *Insight-Non-Destr. Test. Cond. Monit.* **2019**, *61*, 187–196. [CrossRef]
17. Kersemans, M.; Verboven, E.; Segers, J.; Hedayatrasa, S.; Paepegem, W.V. Non-Destructive Testing of Composites by Ultrasound, Local Defect Resonance. In Proceedings of the 18th International Conference on Experimental Mechanics, Brussels, Belgium, 1–5 July 2018. [CrossRef]
18. Hecht, A. Time of Flight Diffraction Technique (TOFD) An Ultrasonic Testing Method for all Applications. *NDT J.* **1997**.
19. Naqiuddin, M.S.M.; Leong, M.S.; Hee, L.M.; Azrieasrie, M.A.M. Ultrasonic signal processing techniques for Pipeline: A review. In Proceedings of the MATEC Web of Conferences, EAAI Conference 2018, Sabah, Malaysia, 3–5 December 2018; Volume 255, p. 06006. [CrossRef]
20. May, Z.; Alam, K.; Nayan, N.A. Recent Advances in Nondestructive Method and Assessment of Corrosion Undercoating in Carbon–Steel Pipelines. *Sensors* **2022**, *22*, 6654. [CrossRef]
21. Kowalczyk, J.; Jósko, M.; Wieczorek, D.; Sędłak, K.; Nowak, M. The Influence of the Hardness of the Tested Material and the Surface Preparation Method on the Results of Ultrasonic Testing. *Appl. Sci.* **2023**, *13*, 9904. [CrossRef]
22. Bourenane, K.; Haddar, A.B.; Haddar, A.; Zerouki, I.; Abdessemed, D. Monitoring and inspection to combat corrosion of pipeline lines in an oil field. *Alger. J. Environ. Sci. Technol.* **2023**, *9*.

23. Hemblade, B. Electrical Resistance Sensor and Apparatus for Monitoring Corrosion. U.S. Patent US 6,946,855 B1, 20 September 2005.

24. Nabil, Y.; Toufik, B.; Morad, G. Ultrasonic TOFD Technique for Cracks Sizing and Locating Based on PSO. In Proceedings of the First International Conference on Electrical Engineering and Advanced Technologies, ICEEAT23, Batna, Algeria, 5–7 November 2023.

25. Gordon, G.A.; Canumalla, S.; Tittmann, B.R. Ultrasonic C-scan imaging for material characterization. *Ultrasonics* **1993**, *31*, 373–380. [CrossRef]

26. Rodriguez, C.; Fernández, M.; Domíngue, J.; Biezma, M.V. Detection of defects in metallic specimens supported by ultrasound propagation simulations. *Mater. Test.* **2014**, *56*, 386–392. [CrossRef]

27. Sainson, S. *Inspection en Ligne des Pipelines—Principes et Méthodes*; Lavoisier: Cachan, France, 2007; p. 332. ISBN 13 978-2-7430-0.

28. DRC Sonatrach Bethioua. Direction of Pipeline Treatment, Online Inspection and Diagnosis by. Group limitedCanada"-PII. 2004.

29. Belmokre, K.; Azzouz, N.; Kermiche, F.; Wery, M.; Pagetti, J. Corrosion study of carbon steel protected by a primer, by electrochemical impedance spectroscopy (EIS) in 3% NaCl medium and in a soil simulating solution. *J. Mater. Corros.* **1998**, *49*, 108–113. [CrossRef]

30. Hansen, N. Hall–Petch relation and boundary strengthening. *Scr. Mater.* **2004**, *51*, 801–806. [CrossRef]

31. Hellier, C. *Handbook of Non—Destructive Evaluations*; Mc Graw-Hill: New York, NY, USA, 2003.

32. Marzorati, S.; Verotta, L.; Trasatti, S.P. green corrosion inhibitors from natural sources and biomass wastes. *Molecules* **2019**, *24*, 48. [CrossRef]

33. Lahrour, S.; Benmoussat, A.; Bouras, B.; Mansri, A.; Tannouga, L.; Marzorati, S. Glycerin-Grafted Starch as Corrosion Inhibitor of C-Mn Steel in 1 M HCl solution. *Appl. Sci.* **2019**, *9*, 4684. [CrossRef]